Comparison of Two-Dimensional and Three-Dimensional Thermal Models of the LENS® Process

H. Yin
Mechanical Engineering Department,
Mississippi State University,
Mississippi State, MS 39762

L. Wang
Center for Advanced Vehicular Systems,
Mississippi State University,
Mississippi State, MS 39762

S. D. Felicelli
Mechanical Engineering Department,
Mississippi State University,
Mississippi State, MS 39762
e-mail: felicelli@me.msstate.edu

A new two-dimensional (2D) transient finite element model was developed to study the thermal behavior during the multilayer deposition by the laser engineered net shaping rapid fabrication process. The reliability of the 2D model was evaluated by comparing the results obtained from the 2D model with those computed by a previously developed three-dimensional (3D) model. It is found that the predicted temperature distributions and the cooling rates in the molten pool and its surrounding area agree well with the experiment data available in literature and with the previous results calculated with the 3D model. It is also concluded that, for the geometry analyzed in this study, the 2D model can be used with good accuracy, instead of the computationally much more expensive 3D model, if certain precautions are taken to compensate for the 3D effects of the substrate. In particular, a 2D model could be applied to an in situ calculation of the thermal behavior of the deposited part during the fabrication, allowing dynamic control of the process. The 2D model is also applied to study the effects of substrate size and idle time on the thermal field and size of the molten pool. [DOI: 10.1115/1.2953236]

1 Introduction

Laser engineered net shaping (LENS®) is a rapid fabrication process, through which near-net-shaped three-dimensional (3D) components are built by the successive overlapping of layers of laser melted powder by the computer-guided movement of the substrate or the laser in 3D space. The LENS fabrication technique was developed by Sandia National Laboratories in the late 1990s and is gaining popularity as a rapid prototyping and repair technology because of its cost saving potentials and high cooling rates leading to fine microstructures similar to those observed in rapid solidification [1–3].

Because the process is not yet fully understood, the selection of process parameters is often based on previous experience and trial and error experimentation. Appropriate tuning of the laser power, travel speed, powder flow rate, and several other parameters is essential to avoid defects and undesired microstructures. Kurz [4], Kelly and Kampe [5], and Colaco and Vilar [6,7], among others, have shown that the microstructure and mechanical properties obtained with the LENS process partly depend on the solid-state transformations during cool down to room temperature. However, the transformations are mainly driven by the consecutive thermal cycles during the LENS process when the laser beam moves along the part surface line by line and layer by layer. Therefore, it is critical to understand the local thermal cycles and temperature history in order to predict the solid phase transformations and thus the final microstructure in the part.

Only a few experimental works have been done to characterize the thermal behavior during LENS deposition [8–13]. Hofmeister et al. [9] employed a digital 64×64 pixel charge coupled device (CCD) video camera with thermal imaging techniques to observe the molten pool. These experiments were conducted on stainless steel 316 (SS316), using two different particle size distributions. The molten pool size was analyzed from the thermal images, and the temperature gradients and cooling rates in the vicinity of the molten pool were also obtained. Griffith et al. [12] inserted a thermocouple directly into the sample to obtain the thermal history during the LENS fabrication. Fine diameter (10 μm) Type C thermocouple wire was used for the measurements to ensure no reaction during deposition, and the thermocouple bead was inserted into the deposition zone for accurate temperature measurements. They obtained in situ temperature data for 20 deposition layers from a representative thermocouple inserted during the fabrication of an H13 tool steel part. Wei et al. [13] employed a two-wavelength imaging pyrometer to capture the thermal images of the stationary molten pool for different laser powers without powder delivery and substrate movement. The thermal images of the moving molten pool were also taken at the beginning state of deposition for two conditions with different laser power and travel velocity settings. The molten pool size, temperature distribution, temperature gradient, and cooling rate in the molten pool were analyzed. It was found that the cooling rate is on the order of 10^2–10^4 K/s in the processed zone.

However, the experimental measurement of a detailed thermal history in the part is difficult to achieve because the required experiments would be very costly and time consuming. An alternative approach is to use numerical simulation with appropriate mathematical models. Several models have been developed to try to establish an understanding of the thermal behavior in the LENS process [14–22]. Grujicic et al. [14,15] developed a two-dimensional (2D) finite element model to calculate the temperature profiles, obtaining the minimum power of the laser needed to initiate the melting of the part surface. Ye et al. [16] developed a finite element model to predict the temperature distribution during the process, especially near the molten pool. Their results showed good agreement with experimental observations. Costa et al. [17] developed and applied a 3D finite element model to calculate the thermal history in a single-wall plate. They also studied the influence of substrate size and idle time on the temperature field of the fabricated parts. Wang and Felicelli [21] predicted the temperature distribution during deposition of SS316 as a function of time and process parameters by developing a 2D thermal model, but only for one layer of deposition. Later, they developed a 3D finite element model [22] using the commercial software SYSWELD to study the molten pool size by analyzing the temperature and phase evolution in stainless steel 410 (SS410) during the LENS deposition of a thin-walled structure.

As with most 3D models, the computational time greatly exceeds that of equivalent 2D models. This is even so when only

Contributed by the Heat Transfer Division of ASME for publication in the JOURNAL OF HEAT TRANSFER. Manuscript received May 24, 2007; final manuscript received January 29, 2008; published online August 8, 2008. Review conducted by Anthony M. Jacobi.

 Copyright © 2008 by ASME

Downloaded 13 Aug 2008 to 130.18.101.156. Redistribution subject to ASME license or copyright; see http://www.asme.org/terms/Terms_Use.cfm

simple heat conduction is being calculated. The computational cost of a 3D model becomes impractical when more complex phenomena of interest are simulated, such as solidification, segregation, porosity, molten pool convection, solid phase transformations, strain and stresses, and others. The single-wall build, in which a thin plate is deposited layer by layer, is the geometry of choice to study the LENS process because of its relative simplicity for modeling and experimental trials. The fact that both 2D and 3D models have been used in literature to simulate this simple geometry indicates that it is not clear whether a 2D model can capture the thermal phenomena of interest. The situation has not been analyzed and, when in doubt, authors resort to 3D modeling at the expense of analysis time and simplified physics. Because the thermal history is the key to predict the microstructure and the mechanical response, the determination of the conditions under which a 2D model can be used to calculate the temperature field with acceptable accuracy would be very useful to undertake combined numerical/experimental studies of the LENS process that go beyond thermal-only aspects.

In the present paper, a 2D finite element model is developed to calculate the temperature distribution during the deposition of multiple layers of SS410. The thermal characteristics and molten pool size predicted with this 2D model is then compared with those calculated with the 3D model developed by Wang et al. [22] and with experimental data. The conditions under which the 2D simulations produce acceptable results are identified, as well as the cases in which 3D effects cannot be captured by the 2D model. The influence of the idle time between the depositions of consecutive layers of material and of substrate size on the thermal cycle/history is also illustrated.

2 Finite Element Mathematical Model

In this section, we describe the 2D finite element model developed to simulate the transient temperature field during the deposition of ten consecutive layers of a single-wall plate of SS410. The schematic of the geometry is shown in Fig. 1(*a*). A fixed finite element mesh is constructed for the substrate and the ten layers of the plate. A uniform layer thickness is used, whose value is set consistently with the powder deposition rate and the travel speed of the laser/nozzle head. Initially, the substrate is at room temperature, and the layer elements are inactive. When a new layer is being deposited, the elements of that layer are activated and they remain active for the rest of the simulation. The boundary conditions (Fig. 1(*b*)) include convection heat loss on the top and sides, a prescribed temperature at the bottom of the substrate, and convection/radiation on the top plus a heat flux due to the incident laser power. The boundary conditions are updated dynamically as layers are activated and new sections of the boundary become active. After finishing depositing one layer and before beginning depositing the next layer, there is a time interval called the idle time, during which the laser/nozzle head is returned to the left end of the plate so that all layers are deposited from left to right. During the idle time, the laser and powder injection are turned off and the corresponding heat flux boundary condition is inactive.

In order to compare the results of the 2D model with those from the 3D model by Wang et al. [22], the same material properties and process parameters are employed. The plate is built by depositing ten layers of material, each with a length of 10.0 mm and a height of 0.5 mm, on top of a substrate with dimensions 5.0 mm high and 10.0 mm long. For comparison purposes, the geometry of the 3D model of Ref. [22] is shown in Fig. 1(*c*). The travel speed of the laser beam is 7.62 mm/s, and the laser beam moves from left to right for each layer deposition. SS410 was used for both the deposited plate layers and the substrate. The thermal properties of SS410 are presented in Table 1, where it is assumed, due to lack of better available data, that the thermal properties of the resolidified SS410 powder are similar to those of the bulk material.

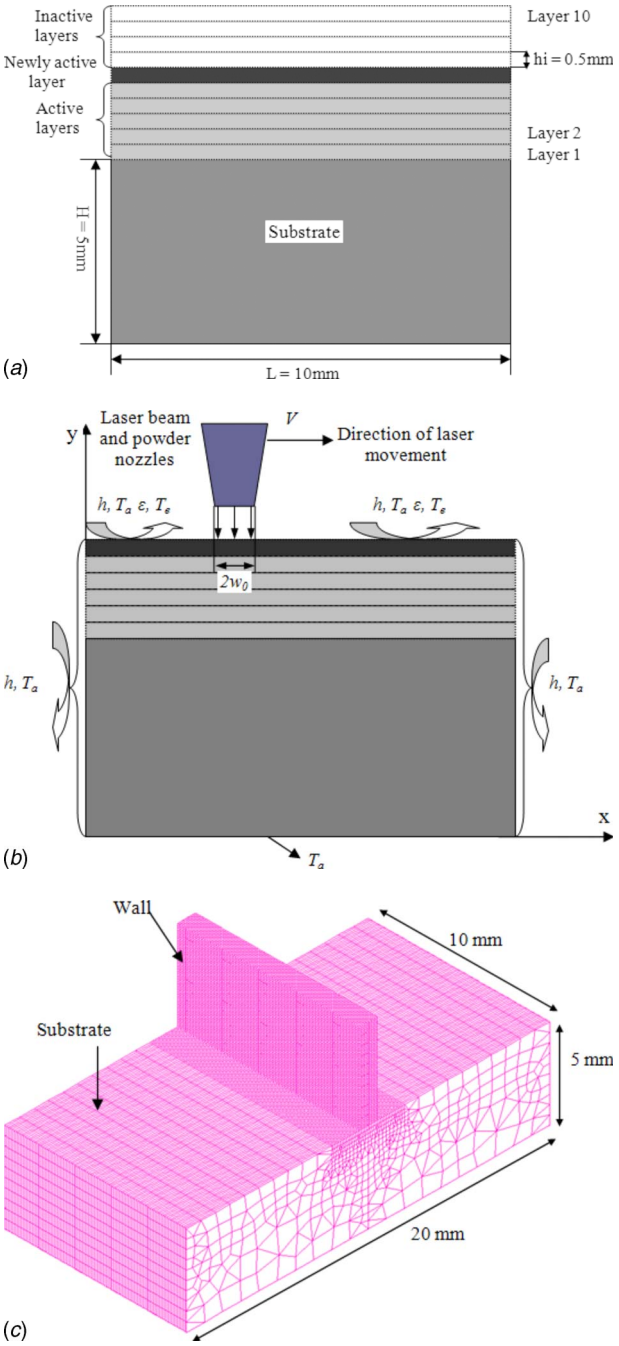

Fig. 1 (*a*) Sketch of the element activation to illustrate the laser powder deposition with multipasses, (*b*) schematic of the model showing the boundary conditions used for the temperature calculation, and (*c*) 3D model of Ref. [22]

2.1 Heat Transfer Equation. The 2D transient equation of heat conduction describing the heat transfer within the plate during the LENS process is

$$\frac{\partial T}{\partial t} = \kappa\left(\frac{\partial^2 T}{\partial x^2} + \frac{\partial^2 T}{\partial y^2}\right) - \frac{L}{C_p}\frac{\partial \phi}{\partial t} \tag{1}$$

where T is the temperature, t is the time, x and y are the horizontal and vertical coordinates, respectively, κ is the thermal diffusivity, L is the latent heat of melting, C_p is the specific heat, and ϕ is the volume fraction of liquid, approximated as $\phi \approx (T-T_s)/(T_l-T_s)$, where T_l is the liquidus temperature and T_s is the solidus temperature of the alloy. This is a reasonable approximation in view of the

Downloaded 13 Aug 2008 to 130.18.101.156. Redistribution subject to ASME license or copyright; see http://www.asme.org/terms/Terms_Use.cfm

Table 1 SS410 thermal properties and LENS process parameters

Parameter	Symbol	Units	Value	Ref.
Density	ρ	kg/m^3	7400	[22]
Thermal conductivity	k	W/m K	25.5	[22]
Specific heat of solid	C_p	J/kg K	650	[22]
Latent heat	L	J/kg	3×10^5	[21]
Liquidus	T_l	K	1723	[21]
Solidus	T_s	K	1693	[21]
Emissivity	ε	N/A	0.8	[21]
Convective heat transfer coefficient	h	W/m^2 K	100	[21]
Radius of the laser beam	w_0	mm	0.5	[21]

very thin mushy zone that forms around the pool [23].

2.2 Initial and Boundary Conditions. The boundary conditions are shown in Fig. 1(*b*). A forced boundary condition is prescribed on the bottom of the substrate:

$$T(x,y,t)|_{y=0} = T_a \tag{2}$$

where T_a is the ambient temperature around the part, in this work considered to be equal to room temperature. The initial temperature of the substrate is also assumed at room temperature,

$$T(x,y,t)|_{t=0} = T_a, \quad y \le H \tag{3}$$

where H is the height of the substrate. The initial condition of the newly deposited material for each layer is set equal to the melting temperature.

$$T(x,y,t)|_{t=0} = T_l, \quad y > H \tag{4}$$

The boundary condition on the section of the top layer under the laser beam is [22]

$$-k\frac{\partial T}{\partial y} = h(T-T_a) + \varepsilon\sigma(T^4 - T_e^4) - Q_r \tag{5}$$

where k is the thermal conductivity, h is the convective heat transfer coefficient, ε is the emissivity of the part surface, σ is the Stefan–Boltzmann constant ($\sigma=5.67\times10^{-8}$ W/m^2 K^4), and T_e is the temperature of the internal wall of the glovebox (taken equal to T_a in this work). In Eq. (5), Q_r is a distributed heat source with a Gaussian profile

$$Q_r = A_0 \exp\left(-\frac{2(x-x_0)^2}{w_0^2}\right) \tag{6}$$

where $A_0=-2\alpha P_1/\sqrt{2\pi}w_0$, being α the effective absorption coefficient of the laser-beam energy, P_l the laser-beam power, w_0 the beam radius, and x_0 the x coordinate of the laser-beam axis.

The boundary condition for the new elements of the top surface, other than the elements beneath the laser beam, considers only the effects of convection and radiation heat loss,

$$-k\frac{\partial T}{\partial y} = h(T-T_a) + \varepsilon\sigma(T^4 - T_e^4) \tag{7}$$

For the two vertical sides, the heat loss due to heat convection is assumed

$$-k\frac{\partial T}{\partial x} = h(T-T_a), \quad x = L \tag{8a}$$

$$+k\frac{\partial T}{\partial x} = h(T-T_a), \quad x = 0 \tag{8b}$$

where L is the width of the plate.

The parameter A_0 in Eq. (6) is used to set the level of power entering the calculation domain. This parameter is necessary because it is not known how much of the nominal laser power is actually absorbed by the material. A similar parameter is used in the 3D model. Because of the limitation of 2D modeling, it is not possible to establish a direct correlation between the actual 3D absorbed power distribution and the idealized 2D power profile used in this work. Ye et al. [20] investigated the thermal behavior in the LENS process with the finite element method. In their work, the temperatures of the nodes where the laser beam focused on were set as the melting point temperatures; thus the laser power did not actually play a role. In this study, the coefficient A_0 is determined by matching the maximum calculated temperature in the molten pool with the measured value reported by Hofmeister et al. [9]. By adjusting A_0, we can calibrate the model to a particular experimental setting. The calibration is done only for one experimental temperature measurement point, then the rest of the temperature profile must result from the model prediction; i.e., A_0 is used to adjust the level of the temperature profile but not the shape of the profile.

By using a 2D model, it is also assumed that there is no significant heat loss through the front and back surfaces of the part. The time evolution of the isotherms is calculated as the laser beam travels across the top surface of the part and layers are deposited. The model dynamically updates the thermal boundary conditions with the laser position and newly added layers; hence it is able to calculate temperature profiles both far from and near the side edges of the plate.

3 Results and Discussions

Due to lack of available experimental data for SS410, we used the experiments of Hofmeister et al. [9] for correlation purposes. In these experiments, ultrahigh speed digital imaging techniques were employed to analyze the image of the molten pool and the temperature gradient on the surface surrounding the molten pool in SS316 samples fabricated using LENS. SS316 and SS410 have similar thermal properties, and in our calculations, we use process parameters (laser power and travel speed) that approximate the conditions of Hofmeister's experiments, in a similar way as it was done in our previous study on the sensitivity of LENS process parameters [21]. To compare the 2D model with the Hofmeister's measurements, a first calculation is performed for the deposition of the top layer (the tenth layer), using the experimental temperature data as the initial condition for the previously built layers.

Figure 2 shows the temperature contours when the laser beam is at the center of the top layer. The travel speed of the laser beam is 7.62 mm/s. It is observed that the temperature profiles predicted by the 2D model (Fig. 2(*a*)) and the 3D model (Fig. 2(*b*)) of Ref. [22] are very similar. Note that the scale of temperature is the same in both figures. The size of the molten pool predicted by the 2D model (Fig. 2(*a*)) is slightly larger than the one predicted by the 3D model (Fig. 2(*b*)) because the heat loss along the z-direction is not considered in the 2D model. Figure 2(*c*) shows the profile of the temperature and cooling rate from the center of the molten pool to a position 4 mm away, opposite to the laser moving direction (indicated in Figs. 2(*a*) and 2(*b*)). The temperature profile calculated by the 2D model qualitatively agrees with the experimental data of Ref. [9] and with the results calculated by the 3D model of Liang et al. [22]. However, the 2D model predicts two small kinks in the temperature and cooling rate curves, which are missed by the 3D model but are consistent with the trend shown in the experiment data. Here by "trend" we mean the qualitative observation that the experimental data show a change in the slope of the temperature and cooling rate profiles at the edge of the molten pool, due to latent heat effect and which is reflected in the 2D model results but not in the 3D (which did not consider latent heat term). The location of these kinks corresponds to a very thin mushy zone surrounding the molten pool and is a consequence of the effect of the latent heat of fusion. The 3D

Downloaded 13 Aug 2008 to 130.18.101.156. Redistribution subject to ASME license or copyright; see http://www.asme.org/terms/Terms_Use.cfm

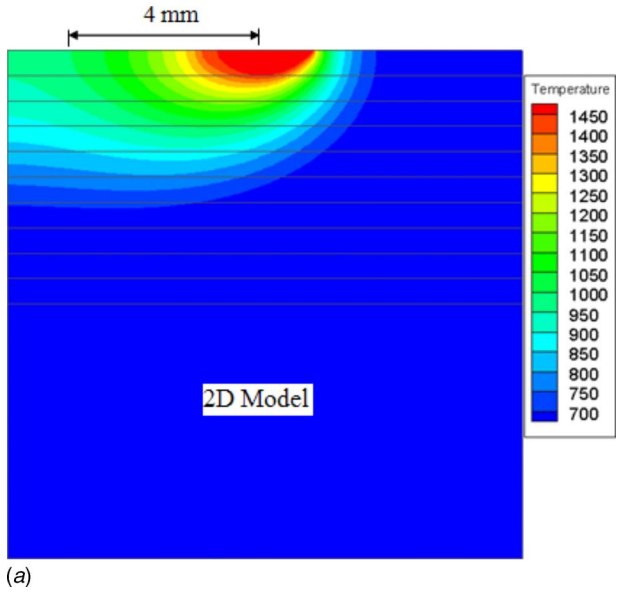

(*a*)

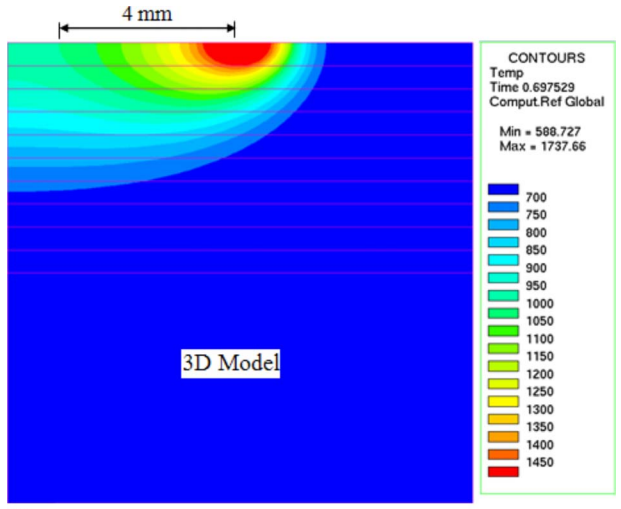

(*b*)

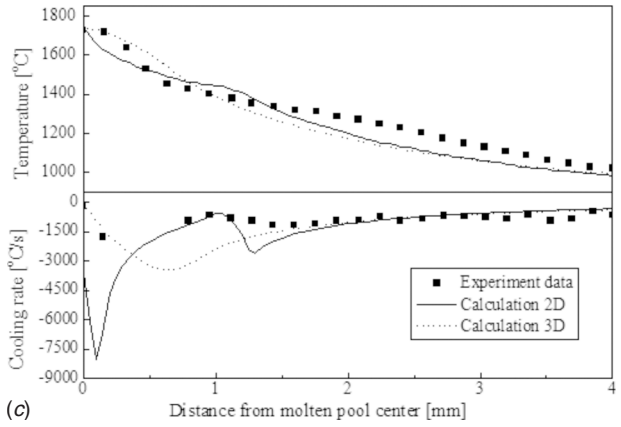

(*c*)

Fig. 2 Temperature distribution predicted (*a*) by the 2D model and (*b*) the 3D mode; molten pool is indicated by the 1450°C isotherm; (*c*) Comparison of calculated results by the 2D and 3D models and experimental data of Hofmeister et al. [9]

model of Ref. [22], based on the commercial software SYSWELD, did not include latent heat effects and hence could not capture this trend.

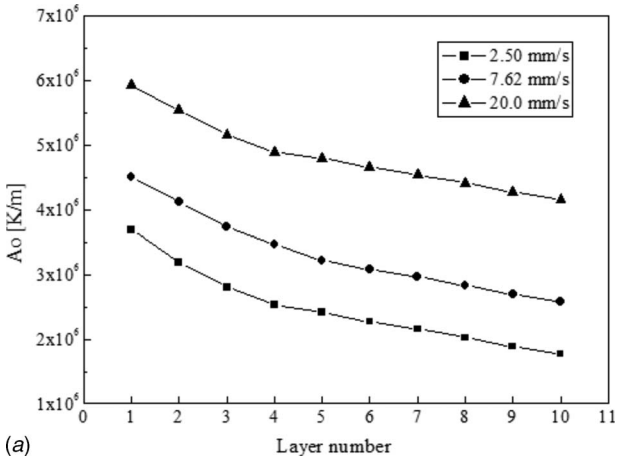

(*a*)

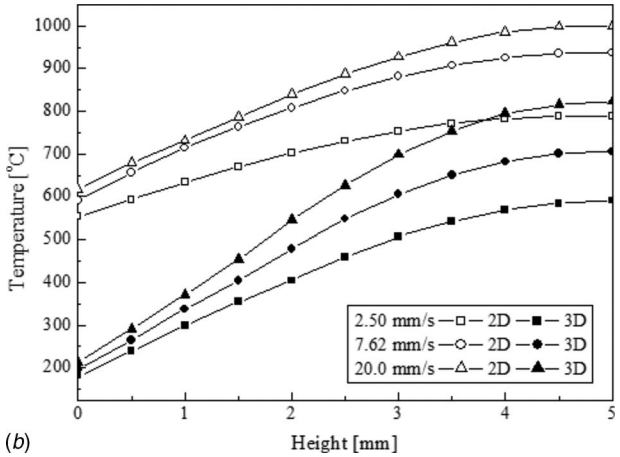

(*b*)

Fig. 3 (*a*) Profiles of the A_0 power coefficient of the 2D model and (*b*) temperature profiles calculated by the 2D and 3D models along the plate centerline for various scanning speeds of the laser beam

In the next simulations, we compare the 2D and 3D models for multilayer deposition for three different travel speeds of the laser beam. In the 3D simulations of Ref. [22], the power program during the deposition of different layers was optimized to obtain a steady molten pool size. In order to reproduce this feature with a 2D model, the power coefficient A_0 needs to be selected accordingly. For each travel speed, the power coefficient A_0 is first determined by matching the maximum temperature in the mid-point of the first layer with the one calculated by the 3D model. For subsequent layers, we assume that A_0 follows the same profile of the power curve of the 3D model, which was optimized for a steady pool size. The A_0—curves for different travel speeds as a function of layer number are shown in Fig. 3(*a*). As explained in Ref. [22], in order to maintain the same pool size from layer to layer, the applied power must decrease as layers are deposited in order to account for the thermal energy storage of the material of the added layers and to compensate for less heat transfer loss to the substrate. The corresponding temperature profiles along the plate centerline, calculated with the 2D and the 3D models, are indicated for three different travel speeds in Fig. 3(*b*), at the time when the tenth layer has been deposited. Higher speeds correspond with higher temperature because less time is available for the layers to cool down between laser scans. In Fig. 3(*b*), we can observe the consequence of having used the same shape of power profile of the 3D part in the 2D calculation. Because the heat loss in the *z*-direction is not considered in the 2D model (and particularly, the heat loss from a 3D substrate), the temperature of the lower portion of the part becomes higher as layers are deposited,

Downloaded 13 Aug 2008 to 130.18.101.156. Redistribution subject to ASME license or copyright; see http://www.asme.org/terms/Terms_Use.cfm

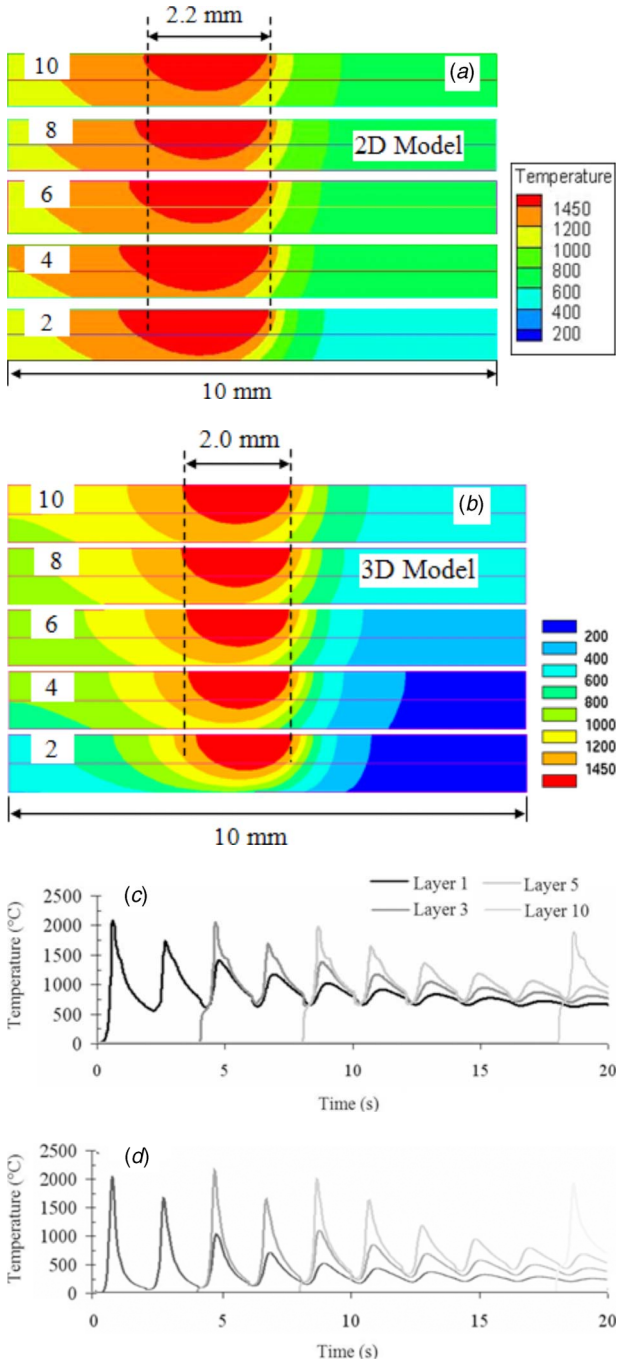

Fig. 4 Temperature distribution when the laser beam is at the center of layers 2, 4, 6, 8, and 10 calculated by the (*a*) 2D and (*b*) 3D models; the molten pool is indicated by the 1450°C isotherm. Temperature cycles at the midpoints of layers 1, 3, 5, and 10 as ten layers are deposited for the (*c*) 2D and (*d*) 3D models. *V*=7.62 mm/s. In (*d*), M_s is the martensite start temperature (350°C).

in comparison with the 3D plate. At the end of the deposition of the tenth layer, the bottom temperature of the 2D plate has increased to 600°C, while the 3D part remained at 200°C. For the upper layers, the temperature is more sensitive to travel speed, but the temperature difference between the 2D and 3D parts becomes less pronounced as the dissipation of the substrate is less dominant.

Figures 4(*a*) and 4(*b*) show the temperature contours in and around the molten pool for Layer Numbers 2, 4, 6, 8, and 10, predicted by the 2D and 3D models, when the laser is at the midpoint of the layer. The laser travel speed is 7.62 mm/s. The molten pool size of the tenth layer is very similar to that predicted by Wang et al. [22]. The discrepancy in pool size between the 2D and 3D models increases as we move down closer to the substrate, as expected from the thermal profiles observed in Fig. 3.

Figure 4(*c*) shows the thermal cycles at the midpoints of deposited Layers 1, 3, 5, and 10 for the 2D model. Figure 4(*d*), extracted from Ref. [22], shows the same cycles calculated with the 3D model. The temperature of each layer reaches a peak every time the laser goes over the midpoint of the plate, and then decreases to a minimum value before the laser starts scanning a new layer (the idle time between layers also affects the minimum temperature). The calculated thermal cycles look similar for the 2D and 3D models, with the discrepancies already observed in Fig. 3, which show higher temperature for the lower layers of the 2D model at the end of the deposition because of the extra heat loss by the 3D substrate. Note also that the cooling part of the cycle curves in the 2D model shows the effect of latent heat, which is missed by the 3D model.

A comparison of the temperature contours predicted by the 2D and 3D models is shown in Fig. 5 for the two other values of travel speed, 2.5 mm/s and 20 mm/s, when the laser is at the midpoint of the tenth layer. It is observed that the molten pool size in this layer is very similar for both 2D and 3D calculations, but the 2D substrate is hotter than the 3D one, the difference being more pronounced for higher travel speed. The elongation effect of the pool for higher speed is similarly captured by the 2D and 3D models.

Figure 6 illustrates the influence of the idle time elapsed between finishing depositing one layer and starting the next layer. Figure 6(*a*) shows the temperature profile along the plate centerline after the tenth layer has been deposited. It is observed that the idle time does not change the shape of the profiles but only displace the curves toward a lower temperature for a longer idle time. The thermal cycles for the case of an idle time of 4.4 s are shown in Fig. 6(*b*). This figure should be compared with Fig. 4(*c*), where the idle time was 0.82 s. It can be seen that a longer idle time allows the midpoint to cool down to a lower temperature, in particular, below the martensite start temperature (350°C). Hence, the idle time can play an important role when trying to control the final microstructure.

The substrate size has an obvious influence on the thermal cycles of depositions. More heat is lost from a larger substrate, which causes a higher temperature gradient along the height of the plate and leads to a lower average temperature. Because of the restricted heat loss in a 2D substrate, increasing the height of the substrate will lead to opposite results, i.e., a higher temperature in the part, if we use a 2D model. This is contrary to the prediction of the 3D model and also opposes the results published by Costa et al. [17]. Actually, in order to approximate the effect of a larger 3D substrate, either the height of the 2D substrate has to be reduced or a lower temperature must be applied as a boundary condition at the bottom of the 2D substrate. The first option is illustrated in Fig. 7 for a travel speed of 7.62 mm/s. Figure 7(*a*) shows the molten pool in different layers for a substrate height of 2 mm. Note the smaller pool size compared with Fig. 4(*a*), in which the substrate height was 5 mm. The temperature profiles along the centerline of the plate are shown in Fig. 7(*b*) for different substrate sizes. Observe that a smaller substrate size tends to better approximate the temperature profiles in Fig. 3(*b*) calculated with the 3D model.

4 Conclusions

A new 2D finite element model was developed to simulate the temperature history during multilayer deposition by the LENS process. This model is an extension of a 2D model previously developed by the authors for one-layer deposition [21]. The objective of the paper was to investigate the applicability of this new

Downloaded 13 Aug 2008 to 130.18.101.156. Redistribution subject to ASME license or copyright; see http://www.asme.org/terms/Terms_Use.cfm

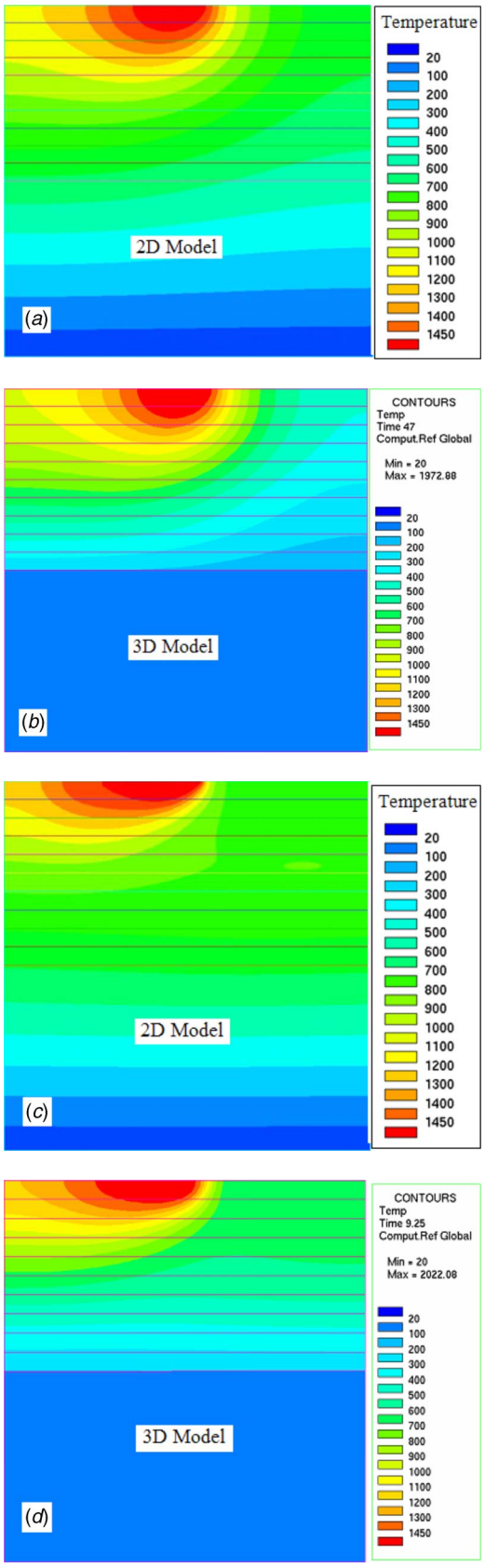

Fig. 5 Temperature distribution when the laser beam is at the center of the tenth layer as predicted by the (*a*) 2D model and (*b*) 3D model for $V=2.50$ mm/s. Temperature distribution when the laser beam is at the center of the tenth layer as predicted by the (*c*) 2D model and (*d*) 3D model for $V=20.0$ mm/s.

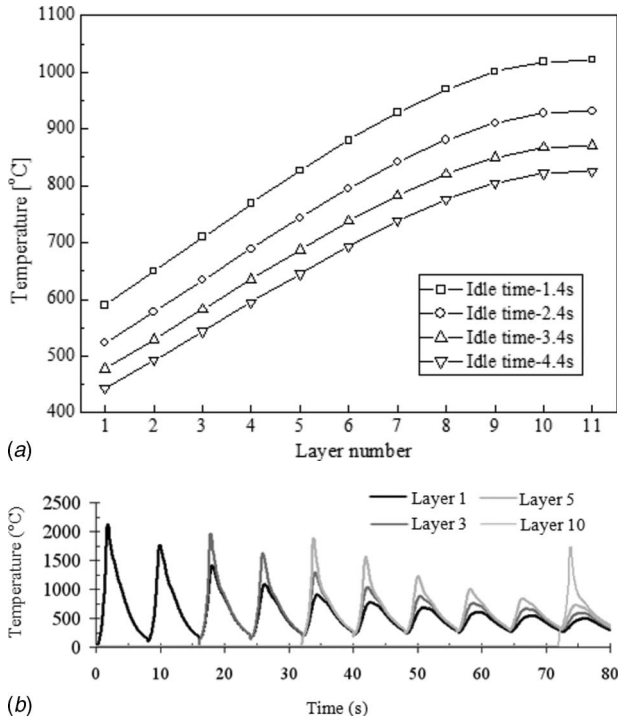

Fig. 6 (*a*) Temperature along the plate centerline for four different idle times after the tenth layer is deposited. (*b*) Temperature cycles at the midpoints of layers 1, 3, 5, and 10 calculated with the 2D model as ten layers are deposited. Idle time is 4.4 s and travel speed $V=2.5$ mm/s.

multilayer model to capture thermal phenomena observed in experiments and previously simulated by a 3D commercial software. The deposition of a thin plate made of ten layers of SS410 built over a substrate of the same material was analyzed. The temperature distribution, temperature history, molten pool size and shape, and cooling rates were calculated with both the 2D and 3D models, comparing the predicted results under variations of process parameters such as laser travel speed, power program, substrate size, and idle time. It was found that the 2D model can reasonably reproduce the results of the 3D model for most cases. It is important to calibrate the power coefficient A_0 of the 2D model so that it reflects an equivalent power level as in a 3D configuration. Also, care must be taken when analyzing the optimization of the power program for steady molten pool size, as well as the effect of changes in the substrate size. Perhaps, the main drawback of the 2D model is that it cannot capture the actual effect of the substrate; hence, 2D and 3D results will differ more pronouncedly in the first deposited layers. A consequent feature is that the 2D model cannot be used, at least in a direct way, to study the effect of different substrate sizes. The higher heat loss produced by a 3D substrate can lead to large discrepancies between the two models, particularly at the lower layers of the part. However, it is possible to design an equivalent 2D model that uses a shorter substrate and produces a thermal response of the part similar to the one observed in the 3D model. Because of the inherent savings in computational time of 2D simulations, more phenomena of interest can be added to a LENS 2D model, such as solidification, pool convection, segregation, and porosity, while still keeping the computational costs at manageable levels. A validated equivalent 2D model can also constitute an improved alternative for online control of the process, which is currently based only on monitoring of the pool size.

Downloaded 13 Aug 2008 to 130.18.101.156. Redistribution subject to ASME license or copyright; see http://www.asme.org/terms/Terms_Use.cfm

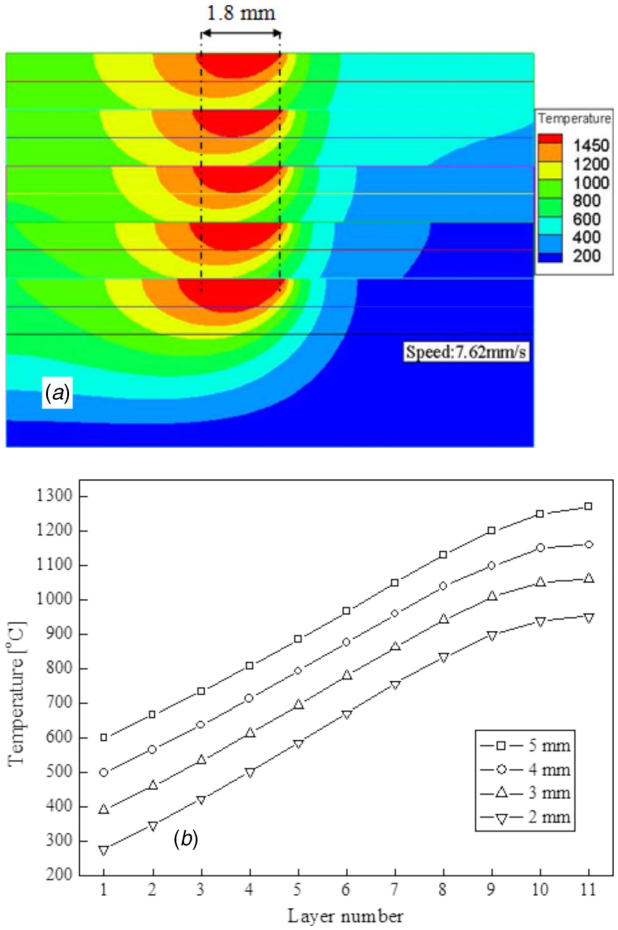

Fig. 7 (*a*) Molten pool size and shape when the laser beam moves to the center of the part for layers 2, 4, 6, 8, and 10, with a substrate height of 2 mm and (*b*) temperature along the plate centerline for four different substrate sizes

Acknowledgment

The authors appreciate the sponsorship of the Center for Advanced Vehicular Systems (CAVS) of Mississippi State University.

Nomenclature

C_p = specific heat
h = convective heat transfer coefficient
H = height of the substrate
k = thermal conductivity
L_0 = width of the plate
L = latent heat of melting
P_l = power of the laser beam
Q_r = distributed heat source with a Gaussian profile
t = time
T = temperature
T_l = liquidus temperature
T_s = solidus temperature
T_a = ambient temperature around the part
T_e = temperature of the internal wall of the glove box
w_0 = radius of the laser beam
x_0 = x coordinate of the laser beam axis
x, y = horizontal and vertical coordinates

Greek Symbols

α = effective absorption coefficient of the laser beam
ε = emissivity of the part surface
κ = thermal diffusivity
ϕ = volume fraction of the liquid
σ = Stefan–Boltzmann constant

References

[1] Atwood, C. L., Griffith, M. L., Schlienger, M. E., Harwell, L. D., Ensz, M. T., Keicher, D. M., Romero, J. A., and Smugeresky, J. E., 1998, "Laser Engineered Net Shaping (LENS®): A Tool for Direct Fabrication of Metal Parts," *Proceedings of ICALEO'98*, Orlando, FL, Nov. 16–19, pp. E-1–E-7.

[2] Lewis, G. K., and Schlienger, M. E., 2003, "Practical Considerations and Capabilities for Laser Assisted Direct Metal Deposition," Mater. Des., **21**, pp. 417–423.

[3] Sears, J. W., 2001, "Solid Freeform Fabrication Technologies: Rapid Prototyping-Rapid Manufacturing," Int. J. Powder Metall., **37**, pp. 417–423.

[4] Kurz, W., 2001, "Solidification Microstructure—Processing Maps: Theory and Application," Adv. Eng. Mater., **3**, pp. 443–452.

[5] Kelly, S. M., and Kampe, S. L., 2004, "Microstructural Evolution in Laser-deposited Multilayer Ti-6A1–4V Builds: Part II. Thermal Modeling," Metall. Mater. Trans. A, **35**, pp. 1869–1879.

[6] Colaco, R., and Vilar, R., 1998, "Effect of the Processing Parameters on the Proportion of Retained Austenite in Laser Surface Melted Tool Steels," J. Mater. Sci. Lett., **17**, pp. 563–567.

[7] Colaco, R., and Vilar, R., 1998, "Effect of Laser Surface Melting on the Tempering Behavior of DIN X42Cr13 Stainless Tool Steel," Scr. Mater., **38**, pp. 107–113.

[8] Hofmeister, W., Griffith, M., Ensz, M., and Smugeresky, J., 2001, "Solidification in Direct Metal Deposition by LENS® Processing," JOM, **53**, pp. 30–34.

[9] Hofmeister, W., Wert, M., Smugeresky, J., Philliber, J., Griffith, M., and Ensz, M., 1999, "Investigation of Solidification in the Laser Engineered Net Shaping (LENS) Process," JOM-e online, **51**(7) www.tms.org/pubs/journals/JOM/9907/Hofmeister/Hofmeister-9907.html.

[10] Griffith, M. L., Ensz, M. T., Puskar, J. D., Robino, C. V., Brooks, J. A., Philliber, J. A., Smugeresky, J. E., and Hofmeister, W. H., 2000, "Understanding the Microstructure and Properties of Components Fabricated by Laser Engineered Net Shaping (LENS)," Mater. Res. Soc. Symp. Proc., **625**, pp. 9–20.

[11] Griffith, M. L., Schlienger, E., Harwell, L. D., Oliver, M. S., Baldwin, M. D., Ensz, M. T., Smugeresky, J. E., Essien, M., Brooks, J., Robino, C. V., Hofmeister, W. H., Wert, M. J., and Nelson, D. V., 1999, "Understanding Thermal Behavior in the LENS™ Process," Mater. Des., **20**, pp. 107–114.

[12] Griffith, M. L., Schlienger, M. E., Harwell, L. D., Oliver, M. S., Baldwin, M. D., Ensz, M. T., Smugeresky, J. E., Essien, M., Brooks, J., Robino, C. V., Hofmeister, W. H., Wert, M. J., and Nelson, D. V., 1998, "Thermal Behavior in the LENS™ Process," *Proceedings of the Solid Freeform Fabrication Symposium*, The University of Texas at Austin, Austin, TX, pp. 89–97.

[13] Wei, W., Zhou, Y., Ye, R. Q., Lee, D., Craig, J. E., Smugeresky, J. E., and Lavernia, E. J., 2002, "Investigation of the Thermal Behavior During the LENS™ Process," *International Conference on Metal Powder Deposition for Rapid Manufacturing*, San Antonio, TX, pp. 128–135.

[14] Grujicic, M., Gao, G., and Figliola, R. S., 2001, "Computer Simulations of the Evolution of Solidification Microstructure in the LENS™ Rapid Function Process," Appl. Surf. Sci., **183**, 43–57.

[15] Grujicic, M., Hu, Y., Fadel, G. M., and Keicher, D. M., 2002, "Optimization of the LENS Rapid Fabrication Process for In-flight Melting of Feed Powder," J. Mater. Synth. Process., **9**, pp. 223–233.

[16] Ye, R., Smugeresky, J. E., Zheng, B., Zhou, Y., and Lavernia, E. J., 2006, "Numerical Modeling of the Thermal Behavior During the LENS Process," Mater. Sci. Eng., A, **428**, pp. 47–53.

[17] Costa, L., Vilar, R., Reti, T., and Deus, A. M., 2005, "Rapid Tooling by Laser Powder Deposition: Process Simulation Using Finite Element Analysis," Acta Mater., **53**, pp. 3987–3999.

[18] Hoadley, A. F. A., and Rappaz, M., 1992, "A Thermal Model of Laser Cladding by Powder Injection," Metall. Trans. B, **23**, pp. 631–642.

[19] Han, L., Liou, F. W., and Phatak, K. M., 2004, "Modeling of Laser Cladding with Powder Injection," Metall. Mater. Trans. B, **35**, pp. 1139–1150.

[20] Ye, R., Zhou, Y., Wei, W., Smugeresky, J. E., and Lavernia, E. J., 2003, "Numerical Modeling of the Thermal Behavior During the LENS Process," *Materials Science and Technology 2003 Meeting*, Chicago, IL, Nov. 9–12, pp. 369–376.

[21] Wang, L., and Felicelli, S., 2006, "Analysis of Thermal Phenomena in LENS™ Deposition," Mater. Sci. Eng., A, **435–436**, pp. 625–631.

[22] Wang, L., Felicelli, S., Gooroochurn, Y., Wang, P. T., and Horstemeyer, M. F., 2008, "Optimization of the LENS™ Process for Steady Molten Pool Size," Mater. Sci. Eng., A, **474**, pp. 148–156.

[23] Faghri, A., and Zhang, Y., 2006, *Transport Phenomena in Multiphase Systems*, Elsevier, New York, p. 460.

Downloaded 13 Aug 2008 to 130.18.101.156. Redistribution subject to ASME license or copyright; see http://www.asme.org/terms/Terms_Use.cfm